AIAA JOURNAL
Vol. 33, No. 10, October 1995

Computational Aeroacoustics: Issues and Methods

Christopher K. W. Tam*
Florida State University, Tallahassee, Florida 32306-3027

Computational fluid dynamics (CFD) has made tremendous progress especially in aerodynamics and aircraft design over the past 20 years. An obvious question to ask is "why not use CFD methods to solve aeroacoustics problems?" Most aerodynamics problems are time independent, whereas aeroacoustics problems are, by definition, time dependent. The nature, characteristics, and objectives of aeroacoustics problems are also quite different from the commonly encountered CFD problems. There are computational issues that are unique to aeroacoustics. For these reasons computational aeroacoustics requires somewhat independent thinking and development. The objectives of this paper are twofold. First, issues pertinent to aeroacoustics that may or may not be relevant to computational aerodynamics are discussed. The second objective is to review computational methods developed recently that are designed especially for computational aeroacoustics applications. Some of the computational methods to be reviewed are quite different from traditional CFD methods. They should be of interest to the CFD and fluid dynamics communities.

Nomenclature

a_0 = speed of sound
D = jet diameter at nozzle exit
$\boldsymbol{e}_r$ = unit vector in the r direction
$\boldsymbol{e}_\theta$ = unit vector in the θ direction
f = frequency
L = core length of a jet
p = pressure
u = velocity component
u_j = jet exit velocity
α = wave number
$\bar{\alpha}$ = wave number of a finite difference scheme
β = wave number in the y direction
Δt = time step
Δx = size of spatial mesh
δ = thickness of mixing layer
λ = acoustic wave length
ν_a = artificial kinematic viscosity
ρ = density
ω = angular frequency
$\bar{\omega}$ = angular frequency of a finite difference scheme
ω_i = imaginary part of the angular frequency

I. Introduction

IT is no exaggeration to say that computational fluid dynamics (CFD) has made impressive progress during the last 20 years, especially in aerodynamics computation. In the hands of competent engineers, CFD has become not only an indispensable method for aircraft load prediction but also a reliable design tool. It is inconceivable that future aircraft would be designed without CFD.

Needless to say, CFD methods have been very successful for the class of problems for which they were invented. An obvious question to ask is "why not use CFD methods to solve aeroacoustics problems?" To answer this question, one must recognize that the nature, characteristics, and objectives of aeroacoustics problems are distinctly different from those commonly encountered in aerodynamics. Aerodynamics problems are, generally, time independent, whereas aeroacoustics problems are, by definition, time dependent. In most aircraft noise problems, the frequencies are very high. Because of these reasons, there are computational issues that are relevant and unique to aeroacoustics. To resolve these issues, computational aeroacoustics (CAA) requires independent thinking and development.

An important point needs to be made at this stage. Computational aeroacoustics is not computational methods alone. If so, it would be called computational mathematics. The application of computational methods to aeroacoustics problems for the purpose of understanding the physics of noise generation and propagation, or for community noise prediction and aircraft certification, is the most important part of CAA. The problem area may be in jet noise, airframe noise, fan and turbomachinery noise, propeller and helicopter noise, duct acoustics, interior noise, sonic boom, or other subfields of aeroacoustics (see Ref. 1 for details). Computational methods are the tools but not the ends of CAA. It is aeroacoustics that defines the area.

As yet there has not been widespread use of computational methods for solving aeroacoustics problems. This paper, therefore, concentrates on discussing the methodology issues in CAA in the hope of stimulating interest in CAA applications and further developments or improvements of computational methods.

The first objective of this paper is to discuss issues pertinent to aeroacoustics that may or may not be relevant to computational aerodynamics. To provide a concrete illustration of these issues, the case of direct numerical simulation of supersonic jet flows and noise radiation will be used. The second objective is to review recently developed computational methods designed especially for CAA applications.

Before one designs a computational algorithm for simulating supersonic jet noise generation and radiation, it is important that one has some idea of the physics of supersonic jet noise. This is extremely important, for any computational scheme would have a finite resolution. This limitation prevents it from being capable of resolving phenomena associated with finer scales of the problem. The principal components of supersonic jet noise are the turbulent mixing noise, the broadband shock-associated noise, and the screech tones.[2,3] In a supersonic jet, the turbulence in the jet flow can be divided into the large-scale turbulence structures/instability waves and the fine-scale turbulence. Both the large turbulence structures and the fine-scale turbulence are noise sources. However, it is known[2,3] that for hot jets of Mach number 1.5 or higher the large turbulence structures/instability waves are responsible for the generation of the dominant part of all of the three principal components of supersonic jet noise. In the discussion that follows, it will be assumed that the noise from fine-scale turbulence, being less important, is ignored. The resolution of fine-scale turbulence is, therefore, not a primary issue.

Received Nov. 1, 1994; presented as Paper 95-0677 at the AIAA 33rd Aerospace Sciences Meeting, Reno, NV, Jan. 9–12, 1995; revision received March 13, 1995; accepted for publication March 15, 1995.

*Professor, Department of Mathematics. Associate Fellow AIAA.

II. Issues Relevant to CAA

To illustrate the various computational issues relevant to CAA, we will consider the case of direct numerical simulation of the generation and radiation of supersonic jet noise by the large turbulence structures/instability waves of the jet flow. Since a computation domain must be finite, it appears that a good choice is to select a domain nearly identical to that in a physical experiment. Figure 1 shows a schematic diagram of a supersonic jet noise experiment inside an anechoic chamber. The exit diameter of the nozzle is a natural length scale of the problem. In order that microphone measurements do provide representative far-field noise data, the lateral wall of the anechoic chamber should be placed not less than 40 diameters from the jet axis. For a high-speed supersonic jet, the centerline jet velocity in the fully developed region of the jet decays fairly slowly, i.e., inversely proportional to the downstream distance. Thus, even at a downstream distance of 50 jet diameters, the jet velocity would still be in the moderately subsonic Mach number range. To avoid strong outflow velocity and to contain all of the noise-producing region of the jet inside the anechoic chamber, it is preferable to have the wall where the diffuser is located to be at least 60 diameters downstream from the nozzle exit. The preceding considerations define the minimum size of the anechoic chamber that will be used as the computational domain.

A. Large Spectral Bandwidth

Jet noise is broadband, and the spectrum is fairly wide. Figure 2 shows a typical noise spectrum of an imperfectly expanded supersonic jet measured by Seiner.[4] The discrete component at the center of the spectrum is the screech tone. The peak to the right of the screech tone is the broadband shock-associated noise. The low-frequency peak to the left is the turbulent mixing noise. The screech tone and the broadband shock-associated noise exist only for imperfectly expanded jets when a quasiperiodic shock cell structure is present in the jet plume. For perfectly expanded jets, the noise consists of turbulent mixing noise alone. Generally, the Strouhal number range (Strouhal number $= fD/u_j$) of interest spans from 0.01 to 10 or a ratio of 10^3 between the highest and the lowest frequency. The spatial resolution requirement of the jet (region A of Fig. 1) is dictated by the sound waves with the shortest wavelengths or the highest frequencies. Typically a minimum of six to eight mesh points per wavelength is required. Suppose one is interested in the turbulent mixing noise of perfectly expanded supersonic jets alone. In this case, the maximum Strouhal number of interest may be taken as 1.0, giving an acoustic wave length λ approximately equal to the jet diameter D. A simple calculation will show that even by using a spatial resolution of only six to eight mesh points per wavelength, the number of mesh points inside the computation domain is enormous. How to develop finite difference algorithms that will give adequate resolution at six to eight mesh points per wavelength is an important issue.

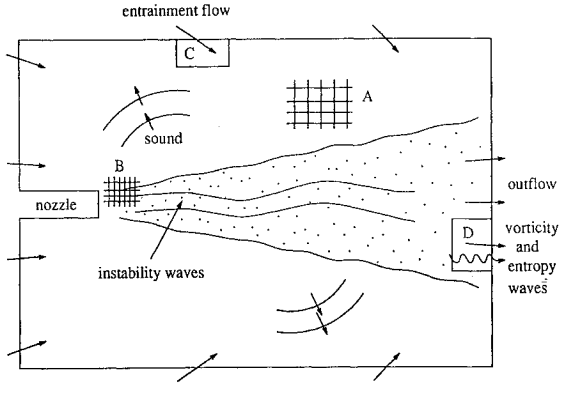

Fig. 1 Schematic diagram showing a supersonic jet noise experiment conducted inside a ventilated anechoic chamber. Not shown are the sound-absorbing wedges on the walls of the chamber. The anechoic chamber is the ideal physical domain for direct numerical simulation.

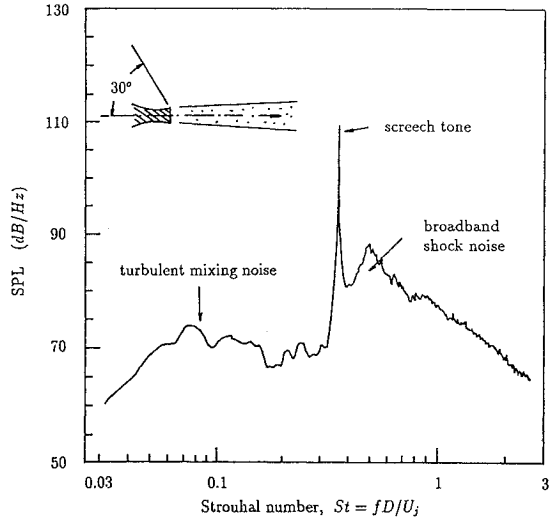

Fig. 2 Typical far-field noise spectrum of an imperfectly expanded supersonic jet, measured at 30-deg inlet angle, showing the three principal noise components. Data from Seiner.[4] Nozzle design Mach number 2.0. Jet Mach number 1.5.

B. Acoustic Wave/Mean Flow Disparity

The root-mean-square velocity fluctuation associated with the radiated sound is usually quite small compared with that of the mean flow of the jet. For example, for a Mach 1.5 jet the measured sound intensity at 40 jet diameters away is around 124 dB. This gives a ratio of sound particle velocity to the jet exit velocity of about 1.5×10^{-4}. That is, the velocity fluctuations of the radiated sound are four orders of magnitude smaller than the mean flow. This large disparity between acoustic and flow variables presents a severe challenge to direct numerical simulation. The small magnitude of the acoustic disturbances can, perhaps, be better appreciated by noting that it is usually smaller than the error (difference between the computed mean flow and the exact mean flow solution) incurred in the computation of the mean flow. This observation led Roe[5] to state that "there is a fear among investigators that the acoustic solutions may be hopelessly corrupted by computational noise." This issue raises the question of whether it is more prudent to solve for the perturbations after the mean flow has first been determined or to solve the full nonlinear equations to capture the very small-amplitude sound field directly. For the jet noise problem, especially for screech tones, the nonlinearity of the problem is crucial to the noise generation process. Thus, there is no alternative but to face the large-magnitude disparity issue.

C. Distinct and Well-Separated Length Scales

Jet noise simulation is an archetypical multilength scale aeroacoustics problem. In the noise source region, the growth and decay of the large turbulence structures/instability waves are controlled locally by the thickness δ of the mixing layer. However, because the flow spreads out in the downstream direction, they are influenced globally by the core length L of the jet. Outside the flow, the natural length scale of the acoustic field is the wave length λ. For most supersonic jets, these various length scales are very distinct and well separated. Typically we have $\delta \ll \lambda < L$. The existence of very disparate length scales calls for careful consideration of the spatial resolution requirement before a direct numerical simulation is attempted. Near the nozzle exit, region B of Fig. 1, the half-width of the mixing layer thickness is usually found to be about 5% of the jet diameter. To resolve adequately the instability waves in the mixing layer of the jet, a minimum of say 15 mesh points are needed. This gives $\Delta r = 0.0033D$ where Δr is the radial mesh spacing in the mixing layer. In the acoustic field, region A of Fig. 1, if sound waves of Strouhal number 1.0 are considered, the mesh spacing required is $\Delta r = D/6$. Thus a spatial resolution of roughly 50 times finer is needed in the sound source region than in the acoustic field. Since numerical instability of most finite difference schemes occurs when the CFL number is larger than a critical value, it follows that the computation time step is dictated by the size of the finest mesh. This, needlessly, leads to excessive CPU time. To make CAA practical,

methods that would overcome the curse of disparate length scales are very much needed.

D. Long Propagation Distance

The quantities of interest in aeroacoustics problems, invariably, are the directivity and spectrum of the radiated sound in the far field. Thus the computed solution must be accurate throughout the entire computation domain. This is in sharp contrast to aerodynamics problems where the primary interest is in determining the loading and moments acting on an airfoil or aerodynamic body. In this class of problems, a solution that is accurate only in the vicinity around the airfoil or body would be sufficient. The solution does not need to be uniformly accurate throughout the entire computation domain.

The distance from the noise source to the boundary of the computation domain is usually quite long. To ensure that the computed solution is uniformly accurate over such long propagation distance, the numerical scheme must be almost free of numerical dispersion, dissipation, and anisotropy. If a large number of mesh points per wavelength are used, this is not difficult to accomplish. However, if one is restricted to the use of only six to eight mesh points per wavelength, the issue is nontrivial. To see the severity of the requirement, let us perform the following estimate for the jet noise problem. Numerical dispersion error is the result of the difference between the group velocities (not the phase velocity as commonly believed) of the waves associated with different wave numbers of the finite difference equations and that of the original partial differential equations. Assume that the computation boundary is at 40 jet diameters away. Let $\bar{\alpha}(\alpha)$ be the wave number of the finite difference scheme (see Sec. III or Ref. 6 for the definition of $\bar{\alpha}$). Then the group velocity of the acoustic waves of the numerical scheme is given by $(\mathrm{d}\bar{\alpha}/\mathrm{d}\alpha)a_0$ (assuming the numerical scheme is dispersion relation preserving). The time needed for the sound wave to propagate to the boundary of the computation domain is $40D/a_0$. Thus, the displaced distance due to numerical dispersion is $[(\mathrm{d}\bar{\alpha}/\mathrm{d}\alpha)a_0 - a_0](40D/a_0)$. If a mesh of six spacings per jet diameter is used and an accumulated numerical displacement less than one mesh spacing is desired, then the slope of the $\bar{\alpha}(\alpha)$ curve of the numerical scheme must satisfy the stringent requirement of

$$\left|\frac{\mathrm{d}\bar{\alpha}}{\mathrm{d}\alpha} - 1\right| \leq \frac{1}{40 \times 6} \tag{1}$$

Most low-order finite difference schemes do not satisfy the preceding condition.

Finite difference schemes, invariably, have built-in numerical dissipation arising from time discretization. This causes a degradation of the computed sound amplitude. Suppose ΔdB is the acceptable numerical error in decibels. Then, it is easy to show that if ω_i is the imaginary part of the angular frequency of the numerical time-marching scheme, this condition can be expressed mathematically[6] as

$$0 > \omega_i \Delta t \geq \frac{1}{240}\left(\frac{\Delta t a_0}{\Delta x}\right) \ell n\left[10^{-\frac{\Delta \mathrm{dB}}{20}}\right] \tag{2}$$

In the case of ΔdB = 1.0 and the Courant–Friedrichs–Lewy number $\Delta t a_0/\Delta x = 0.25$, it is straightforward to find $\omega_i \Delta t \geq -1.2 \times 10^{-4}$. Very few time-marching schemes can meet this demanding requirement.

E. Radiation and Outflow Boundary Conditions

A computation domain is inevitably finite in size. Because of this, radiation and outflow boundary conditions are required at its artificial boundaries. These boundary conditions allow the acoustic and flow disturbances to leave the computation domain with minimal reflection. Again let us consider the problem of direct numerical simulation of jet noise radiation from a supersonic jet as shown in Fig. 1. The jet entrains a significant amount of ambient fluid so that unless the computation domain is very large, there will be nonuniform time-independent inflow at its boundaries. At the same time, the jet flow must leave the computation domain through some part of its boundary. Along this part of the boundary, there is a steady outflow. It is well known that the Euler equations support three types of small-amplitude disturbances. They are the acoustic, the vorticity, and entropy waves. Locally, the acoustic waves propagate at a velocity equal to the vector sum of the acoustic speed and the mean flow velocity. The vorticity and entropy waves, on the other hand, are convected downstream at the same speed and direction as the mean flow. Thus, radiation boundary conditions are required along boundaries with inflow to allow the acoustic waves to propagate out of the computation domain as in region C of Fig. 1. Along boundaries with outflow such as region D of Fig. 1, a set of outflow boundary conditions is required to facilitate the exit of the acoustic, vorticity, and entropy disturbances.

F. Nonlinearities

Most aeroacoustics problems are linear. The supersonic jet noise problem is an exception. It is known experimentally when the jet is imperfectly expanded, strong screech tones are emitted by the jet. The intensity of screech tones around the jet can be as high as 160 dB. At this high intensity, nonlinear distortion of the acoustic waveform is expected. However, because of the three-dimensional spreading of the wave front, experimental measurements inside anechoic chambers do not indicate the formation of shocks. Thus, in the acoustic field, a shock-capturing scheme is not strictly required.

Although there are no acoustic shocks, inside the plume of an imperfectly expanded jet, shocks and expansion fans are formed. These shocks are known to be responsible for the generation of screech tones and broadband shock noise.[2,3] These shocks are highly unsteady. The use of a good shock-capturing scheme that does not generate spurious numerical waves by itself is, therefore, highly recommended in any direct numerical simulation of noise from shock-containing jets.

G. Wall Boundary Conditions

The imposition of wall boundary conditions are necessary whenever there are solid surfaces present in a flow or sound field. Accurate wall conditions are especially important for interior problems such as duct acoustics and noise from turbomachinery. For the supersonic jet noise problem, solid wall boundary conditions are needed to simulate the presence of the nozzle as shown in Fig. 1.

It is easy to see, unless all of the first-order spatial derivatives of the Euler equations are approximated by first-order finite differences, the order of the resulting finite difference equations would be higher than the original partial differential equations. With higher order governing equations, the number of boundary conditions required for a unique solution is larger. In other words, by using a high-order finite difference scheme, an extended set of wall boundary conditions must be developed. The set of physical boundary conditions, appropriate for the original partial differential equations, is no longer sufficient. Aside from the need for extraneous boundary conditions, the use of high-order equations implies the generation of spurious numerical solutions near wall boundaries. In the literature, the question of wall boundary conditions for high-order schemes appears to have been overlooked. The challenge here is to find ways to minimize the contamination of the unwanted numerical solutions generated at the wall boundaries.

III. Computation of Linear Waves

Recently, a number of finite difference schemes[6–9] has been proposed for the computation of linear waves. Numerical experiments and analytical results indicate that only high-order schemes are capable of calculating linear waves with a spatial resolution of six to eight mesh points per wavelength. The high-order essentially nonoscillatory (ENO)[10] and the dispersion-relation-preserving (DRP)[6] schemes are two such algorithms. The ENO scheme is well known. Here we will discuss the DRP scheme and in doing so introduce a few concepts that are new to CFD. The DRP scheme was designed so that the dispersion relation of the finite difference scheme is (formally) the same as that of the original partial differential equations. According to wave propagation theory,[11] this would ensure that the wave speeds and wave characteristics of the finite difference equations are the same as those of the original partial differential equations.

A. Wave Number of a Finite Difference Scheme

Suppose a seven-point central difference is used to approximate the first derivative $\partial f/\partial x$ at the ℓth node of a grid with spacing Δx; i.e.,

$$\left(\frac{\partial f}{\partial x}\right)_\ell \simeq \frac{1}{\Delta x}\sum_{j=-3}^{3} a_j f_{\ell+j} \tag{3}$$

Equation (3) is a special case of the following finite difference equation with x as a continuous variable:

$$\frac{\partial f}{\partial x}(x) \simeq \frac{1}{\Delta x}\sum_{j=-3}^{3} a_j f(x + j\Delta x) \tag{4}$$

The Fourier transform of Eq. (4) is

$$i\alpha \tilde{f} \simeq \left(\frac{1}{\Delta x}\sum_{j=-3}^{3} a_j e^{ij\alpha\Delta x}\right)\tilde{f} \tag{5}$$

where $\tilde{}$ denotes the Fourier transform. By comparing the two sides of Eq. (5), it is evident that the quantity

$$\bar{\alpha} = \frac{-i}{\Delta x}\sum_{j=-3}^{3} a_j e^{ij\alpha\Delta x} \tag{6}$$

is effectively the wave number of the finite difference scheme Eq. (4) or Eq. (3). Tam and Webb[6] suggested to choose coefficients a_j so that Eq. (3) is accurate to order $(\Delta x)^4$ when expanded in Taylor series. The remaining unknown coefficient is chosen so that $\bar{\alpha}$ is a close approximation of α over a wide band of wave numbers. This can be done by minimizing the integrated error

$$E = \int_{-\eta}^{\eta} |\bar{\alpha}\Delta x - \alpha\Delta x|^2 d(\alpha\Delta x) \tag{7}$$

Tam and Shen[12] recommended to set $\eta = 1.1$. The numerical values of a_j determined this way are given in the Appendix together with the coefficients for backward difference stencils. Backward difference stencils are needed at the boundaries of the computation domain.

Figure 3 shows the relation $\bar{\alpha}\Delta x$ vs $\alpha\Delta x$. Over the range $\alpha\Delta x$ up to 1.0 the curve is nearly the same as the straight line $\bar{\alpha} = \alpha$. Figure 4 shows the slope $d\bar{\alpha}/d\alpha$ as a function of $\alpha\Delta x$. Clearly $d\bar{\alpha}/d\alpha$ is close to 1.0 (within 0.3%) up to $\alpha\Delta x = 0.9$ (or seven mesh points per wavelength). This satisfies the requirement of Eq. (1). The standard

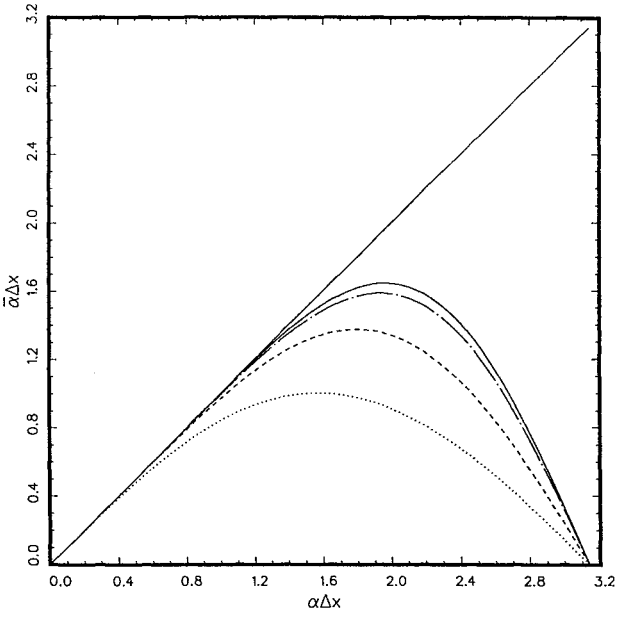

Fig. 3 $\bar{\alpha}\Delta x$ vs $\alpha\Delta x$ relation for the standard central difference second order, · · · · · · · · ·; fourth order, - - - - -; sixth order, — · —; and the DRP scheme, ——.

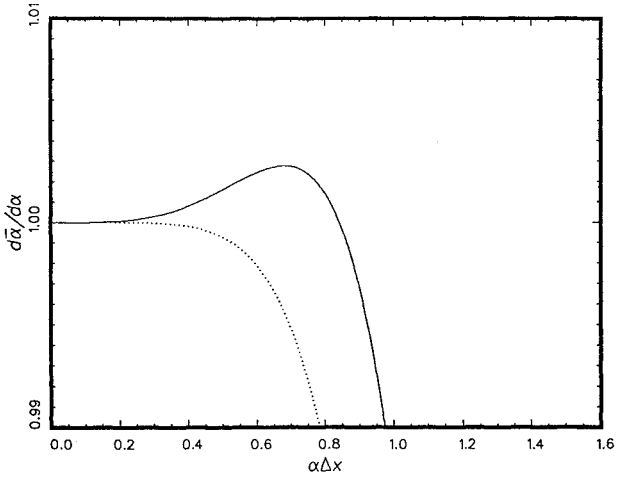

Fig. 4 $d\bar{\alpha}/d\alpha$ vs $\alpha\Delta x$ for the DRP scheme, ——; and the sixth-order standard central difference scheme, · · · · · · · · ·.

sixth-order scheme can resolve waves up to $\alpha\Delta x = 0.6$ (10.5 mesh points per wavelength). There is, therefore, an obvious advantage in using the DRP scheme.

B. Angular Frequency of a Finite Difference Scheme

For time discretization, Ref. 6 proposed to use the following four levels marching scheme:

$$f^{(n+1)} - f^{(n)} = \Delta t\sum_{j=0}^{3} b_j\left(\frac{df}{dt}\right)^{(n-j)} \tag{8}$$

where the superscript indicates the time level. The Laplace transform of Eq. (8) with zero initial condition (for nonzero initial condition, see Ref. 6) yields

$$-i\frac{i(e^{-i\omega\Delta t} - 1)}{\Delta t\sum_{j=0}^{3} b_j e^{ij\omega\Delta t}}\tilde{f} = \widetilde{\frac{df}{dt}} \tag{9}$$

where $\tilde{}$ represents Laplace transform. The Laplace transform of the time derivative, i.e., the right side of Eq. (9), is equal to $-i\omega\tilde{f}$. On comparing the two sides of Eq. (9), the quantity

$$\bar{\omega} = \frac{i(e^{-i\omega\Delta t} - 1)}{\Delta t\sum_{j=0}^{3} b_j e^{ij\omega\Delta t}} \tag{10}$$

is identified as the effective angular frequency of the time marching scheme (8). The coefficients b_j are determined by requiring Eq. (8) to be second order accurate. Tam and Webb[6] found the remaining coefficient by minimizing a weighted integral error, which forces $\bar{\omega}$ to be a good approximation of ω. The numerical values of b_j are given in the Appendix.

For a given value of $\bar{\omega}\Delta t$, Eq. (10) yields four roots of $\omega\Delta t$. In order that the scheme is numerically stable, all of the roots must have a negative imaginary part. Numerical investigations reveal that this is true as long as $\bar{\omega}\Delta t$ is less than 0.4. Hence by choosing a sufficiently small Δt, the scheme is stable. A detailed discussion of the numerical stability of the DRP scheme is provided in Ref. 6. The numerical dissipation rate of the finite difference scheme is given by the imaginary part of ω. By means of Eq. (10) it is, therefore, possible to estimate a priori, for a particular choice of the time step Δt, the amount of numerical damping that would occur (see Ref. 6). This information is most valuable in the design of computer codes.

C. Group Velocity and Numerical Dispersion

The DRP scheme was formulated so that the forms of the dispersion relations are preserved in the discretization process. For the linearized Euler equations, the dispersion relations for the acoustic waves in two dimensions in the absence of a mean flow are

$$\omega = \pm a_0(\alpha^2 + \beta^2)^{\frac{1}{2}} \tag{11}$$

The corresponding dispersion relations for the DRP scheme are [obtained by replacing ω, α, and β by $\bar{\omega}$, $\bar{\alpha}$, and $\bar{\beta}$ in Eq. (11)]

$$\bar{\omega}(\omega) = \pm a_0[\bar{\alpha}^2(\alpha) + \bar{\beta}^2(\beta)]^{\frac{1}{2}} \tag{12}$$

The group velocity[11] of the acoustic waves of the DRP scheme can be obtained by differentiating Eq. (12) with respect to α and β. It is straightforward to find

$$\left(\frac{\partial\omega}{\partial\alpha}, \frac{\partial\omega}{\partial\beta}\right) = \frac{\pm a_0}{(\bar{\alpha}^2 + \bar{\beta}^2)^{\frac{1}{2}}(\mathrm{d}\bar{\omega}/\mathrm{d}\omega)}\left(\bar{\alpha}\frac{\mathrm{d}\bar{\alpha}}{\mathrm{d}\alpha}, \bar{\beta}\frac{\mathrm{d}\bar{\beta}}{\mathrm{d}\beta}\right) \tag{13}$$

If a small Δt is used in the computation, then $\bar{\omega} \simeq \omega$ so that $(\mathrm{d}\bar{\omega}/\mathrm{d}\omega) \simeq 1.0$. For plane acoustic waves propagating in the x direction ($\beta = 0$), the wave velocity given by Eq. (13) reduces to

$$\frac{\partial\omega}{\partial\alpha} = \pm a_0\frac{\mathrm{d}\bar{\alpha}}{\mathrm{d}\alpha} \tag{14}$$

It is clear from Eq. (14) and Fig. 4 that different wave numbers will propagate at different speeds. The dispersiveness of a numerical scheme is, therefore, dependent largely on the slope of the numerical wave number curve. For the seven-point DRP scheme, $\mathrm{d}\bar{\alpha}/\mathrm{d}\alpha$ deviates increasingly from 1.0 for $\alpha\Delta x > 1.0$ (see Fig. 4). The wave speed of the short waves (high wave number) is not equal to a_0. In fact, for the ultrashort waves ($\alpha\Delta x \simeq \pi$) with wavelengths of about two mesh spacings (grid-to-grid oscillations) the group velocity is negative and highly supersonic. The short waves are spurious numerical waves. Once excited they would contaminate and degrade the numerical solution.

To illustrate the effect of numerical dispersion, let us consider the solution of the wave equation

$$\frac{\partial u}{\partial t} + \frac{\partial u}{\partial x} = 0 \tag{15}$$

with initial condition $t = 0$ and $u = e^{-\ln 2(x/3\Delta x)^2}$. Figure 5 shows the computed results of the seven-point DRP scheme, the standard fourth- and sixth-order central difference schemes. The Fourier transform of the initial data is a Gaussian with the main part of the spectrum lying in the range $\alpha\Delta x \leq 1.0$. Thus the DRP scheme can provide adequate resolution for this problem. The group velocity of the wave components in the range $0.8 < \alpha\Delta x < 1.0$ of the sixth-order scheme is considerably less than a_0. This part of the computed waves lags behind the main pulse as shown in Fig. 5. The fourth-order scheme becomes quite dispersive for $\alpha\Delta x > 0.6$. The computed result exhibits large-amplitude trailing waves. In general, low-order schemes are more likely to be affected by numerical dispersion.

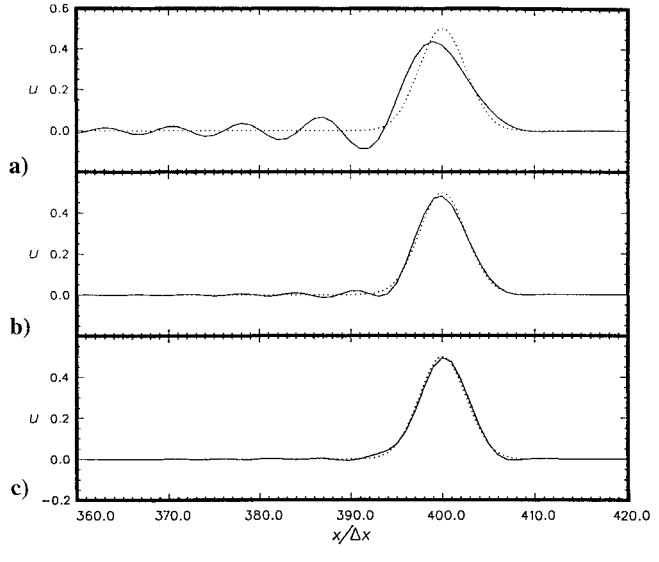

Fig. 5 Comparison between the computed and the exact solutions of the simple one-dimensional wave equation; ——, numerical solution; · · · · · · · · ·, exact solution: a) fourth-order central difference scheme, b) sixth-order central difference scheme, and c) DRP scheme (seven-point stencil).

D. Artificial Selective Damping

To obtain a high-quality numerical solution, it is necessary to eliminate the short wavelength spurious numerical waves. This can be done by introducing artificial selective damping terms in the finite difference equations. The idea of using artificial damping terms to smooth out the profile of a shock is not new.[13,14] Tam et al.[15] refine the idea by developing a way to tailor the damping terms specifically for eliminating only the short waves. For their damping scheme, the long waves ($\alpha\Delta x < 1.0$) are effectively untouched.

Consider the linearized u-momentum equation discretized on a mesh of spacing Δx. Suppose a linear damping term consisting of all of the values of u in the seven-point stencil is added to the right side of the equation. At the ℓth mesh point, the discretized equation may be written as

$$\frac{\mathrm{d}u_\ell}{\mathrm{d}t} + \cdots = -\frac{\nu_a}{(\Delta x)^2}\sum_{j=-3}^{3} d_j u_{\ell+j} \tag{16}$$

where $[\nu_a/(\Delta x)^2]$ is the damping coefficient. The Fourier transform of Eq. (16) is

$$\frac{\mathrm{d}\tilde{u}}{\mathrm{d}t} + \cdots = -\frac{\nu_a}{(\Delta x)^2}D(\alpha\Delta x)\tilde{u} \tag{17}$$

where

$$D(\alpha\Delta x) = \sum_{j=-3}^{3} d_j e^{-ij\alpha\Delta x} \tag{18}$$

Equations (17) and (18) show that the amount of damping depends on the wave numbers so that by choosing the various d_j properly one can damp only the short waves. A way to choose d_j is proposed in Refs. 12 and 15. In the Appendix, a set of values of d_j so obtained is provided. The damping curve $D(\alpha\Delta x)$ vs $\alpha\Delta x$ is shown in Fig. 6. There is practically no damping for long waves ($\alpha\Delta x < 1.0$). Also shown in this figure are the damping curves for the five- and three-point stencils. These smaller stencils are needed at the boundary points where a seven-point stencil would not fit.

To show the effectiveness of the artificial selective damping terms, let us again consider the numerical solution of wave equation (15). But this time, we choose a discontinuous "box-car" initial condition, i.e.,

$$t = 0, \qquad u = 0.5[H(x + 50) - H(x - 50)] \tag{19}$$

where $H(x)$ is the unit step function. Figure 7a shows the computed result at $t = 200(\Delta x/a_0)$ without artificial damping terms.

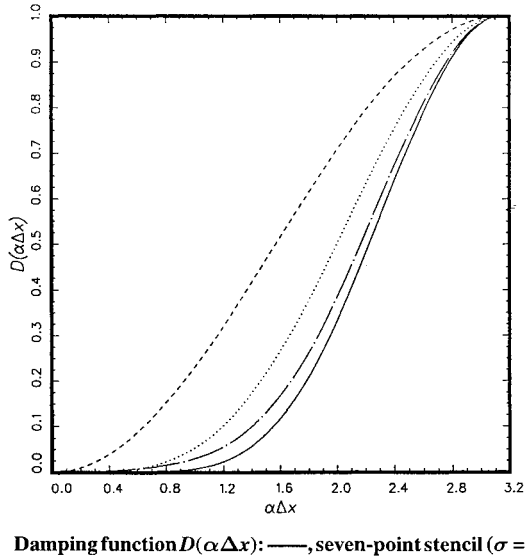

Fig. 6 Damping function $D(\alpha\Delta x)$: ——, seven-point stencil ($\sigma = 0.2\pi$); — · —, seven-point stencil ($\sigma = 0.3\pi$); · · · · · · · · ·, five-point stencil; - - - - -, three-point stencil.

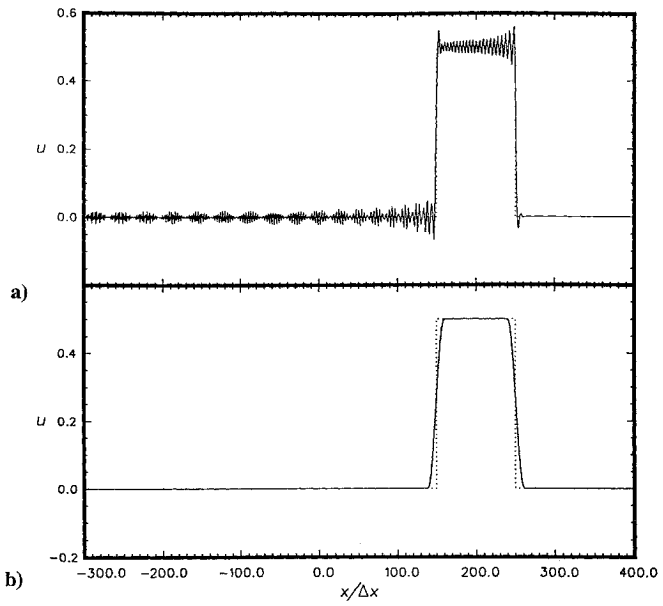

Fig. 7 Waveform initiated by a disturbance with a box-car profile showing parasite waves and the effect of artificial selective damping: a) no artificial damping and b) with artificial damping.

The spurious waves of the computed solution are generated by the discontinuities of the initial condition. The grid-to-grid oscillations have the highest group velocity. They are found to the left of the velocity pulse because their group velocity is negative ($d\bar{\alpha}/d\alpha < 0$). Figure 7b shows the computed solution with artificial damping terms[12] ($R_{\text{stencil}} = 0.05$). Obviously the spurious short waves are largely removed. The quality of the computed solution has greatly improved.

IV. Radiation and Outflow Boundary Conditions

In the past, the subject of radiation boundary conditions has been studied by numerous investigators. One group of investigators used asymptotic solutions to construct radiation boundary conditions. These investigators include Bayliss and Turkel,[16,17] Hagstrom and Hariharan,[18] Hariharan et al.,[19] and Tam and Webb,[6] to mention a few. Another group used the idea of characteristics. These investigators include Thompson,[20,21] Giles,[22] and Poinsot and Lele.[23] Still another group devised ways to construct absorbing boundary conditions to minimize the reflection of waves off the artificial boundary of the computation domain. Investigators of this group are Engquist and Majda,[24,25] Higdon,[26,27] Jiang and Wong,[28] and Kosloff and Kosloff.[29] Recently, Givoli[30] wrote a review article on this subject with extensive references. However, the vast majority of the referenced works are devoted to the simple wave equation. Since the Euler equations, unlike the simple wave equation, support not only acoustic but also vorticity and entropy waves, only a small subset of the aforementioned references are relevant to outflow boundary conditions.

The formulation of radiation and outflow boundary conditions by means of the asymptotic solutions of the problem (strictly speaking, they should be the asymptotic solutions of the finite difference equations[31]) is quite straightforward. Here, the asymptotic solutions model the numerical solution outside the computation domain. For example, consider the problem of sound transmission through a one-dimensional variable area duct as shown in Fig. 8. Upstream of the computation domain, it will be assumed that the duct has a constant area carrying a subsonic mean flow $\bar{u}$, pressure $\bar{p}$, and density $\bar{\rho}$. The fact that the duct has constant area implies the existence of asymptotic solutions valid all of the way to $x \to -\infty$. In this region, the governing equations are the linearized Euler equations:

$$\frac{\partial}{\partial t}\begin{bmatrix}\rho\\ u\\ p\end{bmatrix} + \frac{\partial}{\partial x}\begin{bmatrix}\rho\bar{u} + \bar{\rho}u\\ u\bar{u} + \dfrac{p}{\bar{\rho}}\\ p\bar{u} + \gamma\bar{p}u\end{bmatrix} = 0 \tag{20}$$

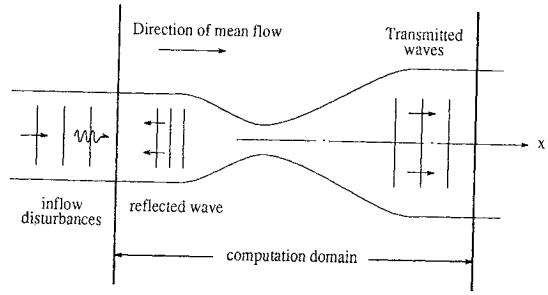

Fig. 8 Schematic diagram of the computation domain for a one-dimensional flow in a variable area duct with constant area terminations. Inflow disturbances at the left boundary consist of sound and entropy waves.

It is easy to show that the general solution of Eq. (20) is

$$\begin{bmatrix}\rho\\ u\\ p\end{bmatrix} = \begin{bmatrix}\dfrac{1}{\bar{a}^2}\\ \dfrac{1}{(\bar{\rho}\bar{a})}\\ 1\end{bmatrix} F\left(\frac{x}{\bar{a}+\bar{u}} - t\right) + \begin{bmatrix}1\\ 0\\ 0\end{bmatrix} G\left(\frac{x}{\bar{u}} - t\right)$$

$$+ \begin{bmatrix}\dfrac{1}{\bar{a}^2}\\ -\dfrac{1}{(\bar{\rho}\bar{a})}\\ 1\end{bmatrix} H\left(\frac{x}{\bar{a}-\bar{u}} + t\right) \tag{21}$$

where F, G, and H are arbitrary functions and $\bar{a} = (\gamma\bar{p}/\bar{\rho})^{1/2}$ is the speed of sound. The solutions associated with the F and G functions are the incoming acoustic and entropy waves. They are known functions at the inflow region. The solution associated with the H function represents the reflected acoustic waves. It is not known a priori. On eliminating H from Eq. (21), the following inflow boundary conditions are derived:

$$\left(\frac{1}{\bar{a}-\bar{u}}\frac{\partial}{\partial t} - \frac{\partial}{\partial x}\right)\begin{bmatrix}\rho\\ u\\ p\end{bmatrix} = -\begin{bmatrix}\dfrac{1}{\bar{a}^2}\\ \dfrac{1}{(\bar{\rho}\bar{a})}\\ 1\end{bmatrix}\frac{2\bar{a}}{\bar{a}^2-\bar{u}^2}$$

$$\times F'\left(\frac{x}{\bar{a}+\bar{u}} - t\right) - \begin{bmatrix}1\\ 0\\ 0\end{bmatrix}\frac{\bar{a}}{\bar{u}(\bar{a}-\bar{u})}G'\left(\frac{x}{\bar{u}} - t\right) \tag{22}$$

In Eq. (22) F' and G' are the derivatives of F and G.

Now, let us return to the supersonic jet noise problem of Fig. 1. Radiation boundary conditions, which allow sound waves to propagate out of the computation domain against the incoming entrainment flow, as well as outflow boundary conditions, which permit an arbitrary combination of acoustic, entropy, and vorticity waves to leave the computation domain smoothly following the jet flow, are needed. The difficulty here is that the mean flow is nonuniform. Tam and Dong[32] recently considered this problem. They proposed the following radiation boundary conditions for two-dimensional time domain computations:

$$\frac{1}{V(r,\theta)}\frac{\partial}{\partial t}\begin{bmatrix}\rho\\ u\\ v\\ p\end{bmatrix} + \frac{\partial}{\partial r}\begin{bmatrix}\rho-\bar{\rho}\\ u-\bar{u}\\ v-\bar{v}\\ p-\bar{p}\end{bmatrix} + \frac{1}{2r}\begin{bmatrix}\rho-\bar{\rho}\\ u-\bar{u}\\ v-\bar{v}\\ p-\bar{p}\end{bmatrix} = 0 \tag{23}$$

where (r, θ) are polar coordinates centered near the middle of the computation domain; $\bar{\rho}$, $\bar{u}$, $\bar{v}$, and $\bar{p}$ are the mean flow quantities at

the boundary region; and $V(r, \theta)$ is related to the mean flow velocity $\boldsymbol{V} = (\bar{u}, \bar{v})$ and the sound speed $\bar{a}$ by

$$V(r, \theta) = \boldsymbol{V} \cdot \boldsymbol{e}_r + \left[\bar{a}^2 - (\boldsymbol{V} \cdot \boldsymbol{e}_\theta)^2\right]^{\frac{1}{2}} \tag{24}$$

For the outflow, they proposed a set of boundary conditions that accounts for mean flow nonuniformity. If the flow is uniform Eq. (23) and the corresponding outflow boundary conditions reduce to those of Tam and Webb,[6] which were derived from the asymptotic solutions of the linearized Euler equations by the method of Fourier transform.

Recently, Hixon et al.[33] tested computationally the effectiveness of the radiation and outflow boundary conditions of Thompson,[20,21] Giles,[22] and Tam and Webb.[6] Their finding was that the boundary conditions based on asymptotic solutions performed well, but the characteristic boundary conditions produced significant reflections. Others also reported similar experience. It is worthwhile to point out that for two- or three-dimensional problems, there are no genuine characteristics. Whenever the waves incident obliquely on the boundary or there is a significant component of mean velocity parallel to the boundary, the validity of any pseudocharacteristic formulation of boundary conditions becomes suspected. Great care should be exercised in their usage.

V. Computation of Nonlinear Acoustic Waves

Nonlinearity causes the waveform of an acoustic pulse to steepen up and ultimately to form a shock. In the study of Tam and Shen,[12] it was found that the nonlinear wave steepening process, when viewed in the wave number space, corresponded to an energy cascade process whereby low wave number components are transferred to the high wave number range. If a high-order finite difference scheme with a large bandwidth of long waves (waves with $\bar{\alpha} \simeq \alpha$) in the wave number space is used for the computation, the computed nonlinear waveform remains accurate as long as the cascading process does not transfer wave components into the unresolved (short) wave number range. Since, in most aeroacoustic problems, the sound intensity is not sufficient to cause the formation of acoustic shocks, the use of a high-order finite difference scheme such as the DRP scheme would generally be quite adequate.

If shocks are formed, it is known that high-order schemes generally produce spurious spatial oscillations around them and in regions with steep gradients. These spurious spatial oscillations are waves in the short wave (high wave number) range generated by the nonlinear wave cascading process. The high-order ENO[10] scheme was conceived and designed to have shock-capturing capability. It should be the method of choice for this type of problem. The ENO schemes, however, automatically perform extensive testing before a finite difference approximation is applied. As a result, it is CPU intensive. If the shock is not very strong, the more straightforward seven-point DRP scheme[12] with artificial selective damping terms added to eliminate the spurious high wave number oscillations around the shock may be used instead. For strong shocks it is necessary to apply the DRP scheme to the governing equations written in conservation form; otherwise the computed shock speed may not be accurate. Figure 9 shows the computed waveform of an acoustic pulse at $t = (40\Delta x/a_0)$ using the seven-point DRP scheme with variable artificial selective damping.[12] Initially the pulse has a Gaussian waveform in u with a half-width equal to $12\Delta x$. As can be seen, the computed waveform compares quite well with the exact solution. The shock, spread over four–five mesh spacings, is not as sharp as those obtained by using specially designed shock-capturing schemes. But this is to be expected.

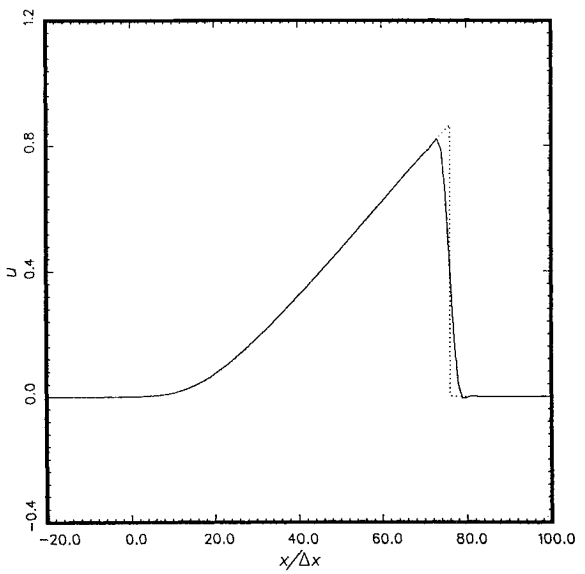

Fig. 9 Computation of a nonlinear acoustic pulse using the DRP scheme with variable artificial damping; $R_{\text{stencil}} = 0.05$, $t = 40\Delta x/a_0$, and Gaussian initial waveform with $u_{\max} = a_0$: ——, numerical solution; ·····, exact solution.

VI. Wall Boundary Conditions

It was pointed out in Sec. II.G that if a high-order finite difference scheme is used to approximate the governing partial differential equations, then the numerical solution is bound to contain spurious components. These spurious solutions can be generated by initial conditions, nonlinearities, and boundary conditions. For example, in the reflection of acoustic waves by a solid wall, the reflected waves would consist of three distinct components.[34] The first component is the reflected wave that closely approximates the exact solution. The second component consists of spurious short waves. Figure 3 shows that there are two (real) values of α for a given $\bar{\alpha}$. The first component corresponds to $\alpha \simeq \bar{\alpha}$. The second component corresponds to the value $\alpha > \bar{\alpha}$. The third component is made up of spatially damped waves. They correspond to the complex roots of α in the $\bar{\alpha}$ vs α relation. For the sound reflection problem, these damped wave solutions are excited by the incident sound waves at the wall. Their amplitudes decay exponentially as they propagate away from the wall. Effectively, they form a numerical boundary layer adjacent to the wall surface.

Figure 10 shows the mesh layout for computing the sound reflection problem. The wall is at $y = 0$. The interior points are points lying three or more rows away from the wall. Their computation stencils lie entirely inside the physical domain. The first three rows of points adjacent to the wall are boundary points. Their seven-point stencils extend outside the physical domain. The points outside the computation domain are ghost points with no obvious physical meaning. However, Tam and Dong[34] observed that ghost points can be useful for the following reason. Recall that the solution of the Euler or Navier–Stokes equations satisfies the partial differential equations at every interior or boundary point. In addition, at a point on the wall the solution also satisfies the appropriate boundary conditions. Now the discretized governing equations are no more than a set of algebraic equations. In the discretized system, each flow variable at either an interior or boundary point is governed by an algebraic equation (discretized form of the partial differential equations). The number of unknowns is exactly equal to the number of equations. Thus there will be too many equations and not enough unknowns if it is insisted that the boundary conditions at the wall are satisfied also. This is, perhaps, one of the major differences between partial differential equations and difference equations. But

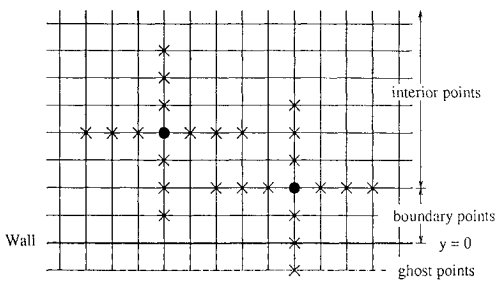

Fig. 10 Mesh layout adjacent to a plane wall showing the interior points, boundary points, and ghost points.

now the extra conditions imposed on the flow variables by the wall boundary conditions can be satisfied if ghost values are introduced (extra unknowns). The number of ghost values is arbitrary, but the minimum number must be equal to the number of boundary conditions. Tam and Dong suggested to use one ghost value per boundary point per physical boundary condition. To eliminate the need for extra ghost values, they employed backward difference stencils to approximate the spatial derivatives at the boundary points. For the plane wall problem, their analysis indicated that the preceding wall boundary treatment would only give rise to very low amplitude spurious reflected waves. The thickness of the numerical boundary layer was also very small regardless of the angle of incidence even when only six mesh points per wavelength were used in the computation.

In most aeroacoustics problems, the wall surface is curved. In CFD, the standard approach is to map the physical domain into a rectangular computational domain with the curved surface mapped into a plane boundary or use unstructured grids. For aeroacoustic problems, this is not necessarily the best method. Mapping or unstructured grids effectively introduce inhomogeneities into the governing equations. Such inhomogeneities could cause unintended acoustic refraction and scattering. An alternative way is to retain a Cartesian mesh and to develop special treatments for curved walls. Kurbatskii and Tam[35] developed one such treatment by extending the one ghost value per boundary point per physical boundary condition of Tam and Dong.[34] They tested their curved wall boundary conditions by solving a series of linear two-dimensional acoustic wave scattering problems. Morris et al.[36] proposed not to use the wall boundary condition. Instead they simulated the change in impedance at the wall by increasing the density of the fluid inside the solid body. At this time, it is too early to judge how well these alternative methods would perform in problems with complex wall boundaries. But for problems involving simple scatterers such as circular and elliptic cylinders, excellent computed results of the entired scattered acoustic field have been obtained.[35] In any case, mapping or unstructured grids may not be absolutely necessary for aeroacoustics problems.

VII. Concluding Remarks

As a subdiscipline, CAA is still in its infancy. In this paper, some of the relevant computational issues and methods are discussed (for a set of benchmark problems designed to address some of these issues see Ref. 37). Obviously, the development of new methods is very much needed. However, it is also pertinent to echo the belief that applications of CAA to important or as yet unsolved aeroacoustics problems are just as needed. It is necessary to demonstrate the usefulness, reliability, and robustness of CAA. Unless and until this is accomplished, CAA will remain merely a research subject but not an engineering tool.

Appendix: Stencil and Damping Coefficients

The coefficients of the seven-point DRP scheme are

$$a_0 = 0 \qquad a_1 = -a_{-1} = 0.770882380518$$
$$a_2 = -a_{-2} = -0.166705904415$$
$$a_3 = -a_{-3} = 0.208431427703$$

Backward stencil coefficients are a_j^{nm}, $j = -n, -n+1, \ldots, m-1$, m (n = number of points to the left and m = number of points to the right):

$$a_0^{06} = -a_0^{60} = -2.192280339 \qquad a_{-1}^{15} = -a_1^{51} = -0.209337622$$
$$a_1^{06} = -a_{-1}^{60} = 4.748611401 \qquad a_0^{15} = -a_0^{51} = -1.084875676$$
$$a_2^{06} = -a_{-2}^{60} = -5.108851915 \qquad a_1^{15} = -a_{-1}^{51} = 2.147776050$$
$$a_3^{06} = -a_{-3}^{60} = 4.461567104 \qquad a_2^{15} = -a_{-2}^{51} = -1.388928322$$
$$a_4^{06} = -a_{-4}^{60} = -2.833498741 \qquad a_3^{15} = -a_{-3}^{51} = 0.768949766$$
$$a_5^{06} = -a_{-5}^{60} = 1.128328861 \qquad a_4^{15} = -a_{-4}^{51} = -0.281814650$$
$$a_6^{06} = -a_{-6}^{60} = -0.203876371 \qquad a_5^{15} = -a_{-5}^{51} = 0.048230454$$

$$a_{-2}^{24} = -a_2^{42} = 0.049041958$$
$$a_{-1}^{24} = -a_1^{42} = -0.468840357$$
$$a_0^{24} = -a_0^{42} = -0.474760914$$
$$a_1^{24} = -a_{-1}^{42} = 1.273274737$$
$$a_2^{24} = -a_{-2}^{42} = -0.518484526$$
$$a_3^{24} = -a_{-3}^{42} = 0.166138533$$
$$a_4^{24} = -a_{-4}^{42} = -0.026369431$$

The coefficients of the four-level time-marching stencil are

$$b_0 = 2.302558088838$$
$$b_1 = -2.491007599848$$
$$b_2 = 1.574340933182$$
$$b_3 = -0.385891422172$$

The coefficients of the seven-point damping stencil are

	$(\sigma = 0.2\pi)$	$(\sigma = 0.3\pi)$
d_0	0.287392842460	0.327698660845
$d_1 = d_{-1}$	−0.226146951809	−0.235718815308
$d_2 = d_{-2}$	0.106303578770	0.086150669577
$d_3 = d_{-3}$	−0.023853048191	−0.014281184692

The coefficients of the five-point damping stencil are

$$d_0 = 0.375$$
$$d_1 = d_{-1} = -0.25$$
$$d_2 = d_{-2} = 0.0625$$

The coefficients of the three-point stencil are

$$d_0 = 0.5, \qquad d_1 = d_{-1} = -0.25$$

Acknowledgments

This work was supported by NASA Lewis Research Center Grant NAG 3-1267. Part of this work was written while the author was in residence at the Institute for Computer Applications in Science and Engineering. The author wishes to thank Hao Shen and David Kopriva for their assistance.

References

[1]Hubbard, H. H. (ed.), *Aeroacoustics of Flight Vehicles: Theory and Practice*, Vol. 1: Noise Sources, Vol. 2: Noise Control, NASA RP-1258, Aug. 1991.

[2]Tam, C. K. W., "Jet Noise Generated by Large-Scale Coherent Motion," *Aeroacoustics of Flight Vehicles*, NASA RP-1258, Aug. 1991, Chap. 6, pp. 311–390.

[3]Tam, C. K. W., "Supersonic Jet Noise," *Annual Review of Fluid Mechanics*, Vol. 27, 1995, pp. 17–43.

[4]Seiner, J. M., "Advances in High-Speed Jet Aeroacoustics," AIAA Paper 84-2275, Oct. 1984.

[5]Roe, P. L., "Technical Prospects for Computational Aeroacoustics," AIAA Paper 92-02-032, May 1992.

[6]Tam, C. K. W., and Webb, J. C., "Dispersion-Relation-Preserving Finite Difference Schemes for Computational Acoustics," *Journal of Computational Physics*, Vol. 107, Aug. 1993, pp. 262–281.

[7]Thomas, J. P., and Roe, P. L., "Development of Non-Dissipative Numerical Schemes for Computational Aeroacoustics," AIAA Paper 93-3382, July 1993.

[8]Zingg, D. W., Lomax, H., and Jurgens, H., "An Optimized Finite Difference Scheme for Wave Propagation Problems," AIAA Paper 93-0459, Jan. 1993.

[9]Lockard, D. P., Brentner, K. S., and Atkins, H. L., "High Accuracy Algorithms for Computational Aeroacoustics," AIAA Paper 94-0460, Jan. 1994.

[10]Harten, A., Engquist, A., Osher, S., and Chakravarthy, S., "Uniformly High-Order Accuracy Essentially Non-Oscillatory Schemes III," *Journal of Computational Physics*, Vol. 71, Aug. 1987, pp. 231–323.

[11]Whitham, G. B., *Linear and Nonlinear Waves*, Wiley-Interscience, New York, 1974.

[12]Tam, C. K. W., and Shen, H., "Direct Computation of Nonlinear Acoustic Pulses Using High-Order Finite Difference Schemes," AIAA Paper 93-4325, Oct. 1993.

[13]Von Neumann, J., and Richtmyer, R. D., "A Method for the Numerical Calculation of Hydrodynamic Shocks," *Journal of Applied Physics*, Vol. 21, March 1950, pp. 232–237.

[14]Jameson, A., Schmidt, W., and Turkel, E., "Numerical Solutions of the Euler Equations by Finite Volume Methods Using Runge–Kutta Time Stepping Schemes," AIAA Paper 81-1259, June 1981.

[15]Tam, C. K. W., Webb, J. C., and Dong, Z., "A Study of the Short Wave Components in Computational Acoustics," *Journal of Computational Acoustics*, Vol. 1, March 1993, pp. 1–30.

[16]Bayliss, A., and Turkel, E., "Radiation Boundary Conditions for Wave-Like Equations," *Communications on Pure and Applied Mathematics*, Vol. 33, Nov. 1980, pp. 707–725.

[17]Bayliss, A., and Turkel, E., "Far Field Boundary Conditions for Compressible Flows," *Journal of Computational Physics*, Vol. 48, Nov. 1982, pp. 182–199.

[18]Hagstrom, T., and Hariharan, S. I., "Accurate Boundary Conditions for Exterior Problems in Gas Dynamics," *Mathematics of Computation*, Vol. 51, Oct. 1988, pp. 581–597.

[19]Hariharan, S. I., Ping, Y., and Scott, J. C., "Time Domain Numerical Calculations of Unsteady Vortical Flows About a Flat Plate Airfoil," *Journal of Computational Physics*, Vol. 101, Aug. 1992, pp. 419–430.

[20]Thompson, K. W., "Time Dependent Boundary Conditions for Hyperbolic Systems," *Journal of Computational Physics*, Vol. 68, Jan. 1987, pp. 1–24.

[21]Thompson, K. W., "Time Dependent Boundary Conditions for Hyperbolic Systems, II," *Journal of Computational Physics*, Vol. 89, Aug. 1990, pp. 439–461.

[22]Giles, M. B., "Nonreflecting Boundary Conditions for Euler Equation Calculations," *AIAA Journal*, Vol. 28, No. 12, 1990, pp. 2050–2058.

[23]Poinsot, T. J., and Lele, S. K., "Boundary Conditions for Direct Simulations of Compressible Viscous Flows," *Journal of Computational Physics*, Vol. 101, July 1992, pp. 104–129.

[24]Engquist, B., and Majda, A., "Radiation Boundary Conditions for Acoustic and Elastic Wave Calculations," *Communications on Pure and Applied Mathematics*, Vol. 32, May 1979, pp. 313–357.

[25]Engquist, B., and Majda, A., "Absorbing Boundary Conditions for the Numerical Simulation of Waves," *Mathematics of Computation*, Vol. 31, July 1977, pp. 629–651.

[26]Higdon, R. L., "Absorbing Boundary Conditions for Difference Approximations to the Multi-Dimensional Wave Equation," *Mathematics of Computation*, Vol. 47, Oct. 1986, pp. 629–651.

[27]Higdon, R. L., "Numerical Absorbing Boundary Conditions for the Wave Equation," *Mathematics of Computation*, Vol. 49, July 1987, pp. 65–90.

[28]Jiang, H., and Wong, Y. S., "Absorbing Boundary Conditions for Second Order Hyperbolic Equations," *Journal of Computational Physics*, Vol. 88, May 1990, pp. 205–231.

[29]Kosloff, R., and Kosloff, D., "Absorbing Boundaries for Wave Propagation Problems," *Journal of Computational Physics*, Vol. 63, April 1986, pp. 363–376.

[30]Givoli, D., "Non-Reflecting Boundary Conditions," *Journal of Computational Physics*, Vol. 94, May 1991, pp. 1–29.

[31]Tam, C. K. W., and Webb, J. C., "Radiation Boundary Condition and Anisotropy Correction for Finite Difference Solutions of the Helmholtz Equation," *Journal of Computational Physics*, Vol. 113, July 1994, pp. 122–133.

[32]Tam, C. K. W., and Dong, Z., "Radiation and Outflow Boundary Conditions for Direct Computation of Acoustic and Flow Disturbances in a Nonuniform Mean Flow," AIAA Paper 95-007, June 1995.

[33]Hixon, D. R., Shih, S., and Mankbadi, R. R., "Evaluation of Boundary Conditions for Computational Aeroacoustics," AIAA Paper 95-0160, Jan. 1995.

[34]Tam, C. K. W., and Dong, Z., "Wall Boundary Conditions for High-Order Finite Difference Schemes in Computational Aeroacoustics," *Theoretical and Computational Fluid Dynamics*, Vol. 8, No. 6, 1994, pp. 303–322.

[35]Kurbatskii, K. A., and Tam, C. K. W., "Curved Wall Boundary Conditions for High-Order Finite Difference Schemes in Acoustic Wave Scattering Problems," *Bulletin of the American Physical Society*, Vol. 39, Nov. 1994, p. 1907.

[36]Morris, P. J., Chung, C., Chyczewski, T. S., and Long, L. N., "Computational Aeroacoustics Algorithms: Nonuniform Grids," AIAA Paper 94-2295, June 1994.

[37]Hardin, J. C. (ed.), *Computational Aeroacoustics Benchmark Problems, Proceeding of the ICASE/LaRC Workshop on Benchmark Problems in Computational Aeroacoustics* (Hampton, VA), NASA CP-3300, May 1995.